

Breit-Wigner-Fano lineshapes in Raman spectra of graphene

Eddwi H. Hasdeo,^{1,*} Ahmad R. T. Nugraha,¹ Mildred S. Dresselhaus,^{2,3} and Riichiro Saito¹

¹*Department of Physics, Tohoku University, Sendai 980-8578, Japan*

²*Department of Electrical Engineering and Computer Science,
Massachusetts Institute of Technology,
Cambridge, Massachusetts 02139-4037, USA*

³*Department of Physics, Massachusetts Institute of Technology,
Cambridge, Massachusetts 02139-4307, USA*

(Dated: August 4, 2018)

Abstract

Excitation of electron-hole pairs in the vicinity of the Dirac cone by the Coulomb interaction gives rise to an asymmetric Breit-Wigner-Fano lineshape in the phonon Raman spectra in graphene. This asymmetric lineshape appears due to the interference effect between the phonon spectra and the electron-hole pair excitation spectra. The calculated Breit-Wigner-Fano asymmetric factor $1/q_{\text{BWF}}$ as a function of the Fermi energy shows a “V”-shaped curve with a minimum value at the charge neutrality point and gives good agreement with the experimental result.

PACS numbers: 78.67.Wj, 73.22.Pr, 42.65.Dr, 03.65.Nk

I. INTRODUCTION

Elementary excitations such as electrons and phonons can be probed by the inelastic scattering of light using the Raman spectroscopy technique. In graphene-related systems, studying the shape of the Raman spectra can give us a deep understanding of the electron energy dispersion,¹ phonon energy dispersion,² lifetime of excitations,³ the Kohn anomaly effect,⁴ and structure characterization.⁵ In particular, the asymmetric Breit-Wigner-Fano (BWF) lineshape, historically observed in the Raman spectra of graphite intercalation compounds (GICs)⁶ and metallic nanotubes (m-SWNTs),⁷ probes interference between the continuum spectra with discrete spectra.⁸ Recently, the BWF asymmetry has been observed by Yoon *et al.*⁹ in monolayer graphene indicating a common origin of the BWF lineshape of the graphite-related systems (i.e. GICs, m-SWNTS, and monolayer graphene) that arise due to the presence of the Dirac cone or linear energy band structure.

The BWF lineshape is defined by the following formula

$$\begin{aligned} I_{\text{BWF}}(\omega_s) &= I_0 \frac{(1 + s/q_{\text{BWF}})^2}{1 + s^2} \\ &= I_0 \left[\frac{1}{q_{\text{BWF}}^2} + \frac{1 - 1/q_{\text{BWF}}^2}{1 + s^2} + \frac{2s/q_{\text{BWF}}}{1 + s^2} \right], \end{aligned} \quad (1)$$

where $s = (\omega_s - \omega_G)/\Gamma$. Here ω_s , ω_G , $1/q_{\text{BWF}}$, Γ , and I_0 are the Raman shift, the spectral peak position, the asymmetric factor, the spectral width, and the maximum intensity of the BWF spectra, respectively. The right hand side of Eq. (1) tells us that the BWF lineshape respectively consists of a constant continuum spectrum, a discrete Lorentzian spectrum, and an interference effect between both spectra. When $1/q_{\text{BWF}} = 0$, Eq. (1) gives a Lorentzian lineshape which represents a discrete phonon spectrum. The interference term gives rise to an asymmetric lineshape for positive and negative values of s , in which the asymmetry is proportional to a dimensionless parameter $1/q_{\text{BWF}}$, mimicking the ratio between the probability amplitude of the continuum spectra to that of the discrete spectra.⁸

In the Raman spectroscopy studies of graphite-related systems,^{10,11} continuum spectra come from the electronic excitations and are usually observed only in metallic systems. The BWF lineshapes in graphene have been found in various kinds of phenomena such as scanning tunneling microscopy,¹² optical conductivity,¹³ photoabsorption spectroscopy,¹⁴ and infrared spectroscopy^{15,16} revealing that electron-hole pair excitations in the vicinity of the Dirac cone play an important role in the continuum spectra.

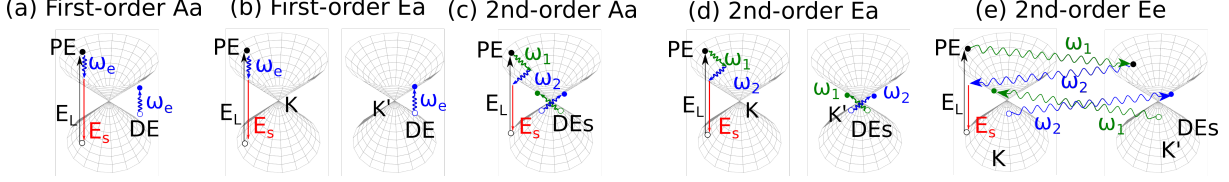


Figure 1: (Color online) All possible Coulomb interactions between a photoexcited electron (PE) and electrons on the Dirac cone (DEs): (a) a first-order intravalley interaction and intravalley scattering (Aa), (b) a first-order intervalley interaction and intravalley scattering (Ea), (c) a second-order intravalley interaction and intravalley scattering (Aa), (d) a second order intervalley interaction and intravalley scattering (Ea), and (e) a second order intervalley interaction and intervalley scattering (Ee). Capital (small) letters A {a} and E {e} label the intravalley and the intervalley interactions {scatterings}. The Raman shift ω_s is the energy difference between laser excitation energy E_L and the scattered photon energy E_s which corresponds to the energy used to excite a DE (DEs) in the first(second)-order processes, $\omega_s = \omega_e$ ($\omega_s = \omega_1 + \omega_2$).

The asymmetric BWF lineshapes in graphite-related systems are normally found in the Raman shift around 1600 cm^{-1} , known as the G modes, which correspond to two zone-center ($\mathbf{q} = 0$) phonon modes, namely the in-plane tangential optic (iTO) and longitudinal optic modes. In graphene, the BWF asymmetry of the G band is observed using the gate-modulated Raman spectroscopy.⁹ The asymmetric factor ($1/q_{\text{BWF}}$) has a value around -0.06 or one-order of magnitude smaller than those found in m-SWNTs ($1/q_{\text{BWF}} \approx -0.4$)⁷ and in GICs ($1/q_{\text{BWF}} \approx -0.5$).⁶ The absolute value of the BWF asymmetric factor greatly decreases as we change the Fermi energy (E_F) to be further from the Dirac point by applying a positive or a negative bias with respect to the charge neutrality point.^{9,17} These results give a clue that the asymmetric factor strongly depends on the electronic density of states (DOS) near the Dirac cone.

In this work, we show that the origin of the BWF spectra in graphene comes from the continuous single particle electron-hole pair spectra, interfering with the discrete phonon spectra. Hereafter, we refer to the single particle electron-hole pair spectra as the electronic Raman spectra (ERS).¹⁸ In the previous work for m-SWNTs, we discuss that the ERS spectra originate from the second-order Coulomb interaction with non-zero momentum transfer $\mathbf{q} \neq 0$, due to the symmetry of the A and B sublattice wavefunctions which gives rise to the absence of the direct Coulomb interaction at the zone center $\mathbf{q} = 0$.¹⁹ Unlike the previous

calculation for m-SWNTs which utilized exciton wavefunctions,¹⁹ in this calculation we use electron wavefunctions from the tight binding (TB) method because our calculation regime (2.4 eV) is far from the saddle point energy dispersion (4 eV), and thus the exciton effects are negligible.^{14,20} The use of electron wavefunctions give considerable contributions of the intervalley scattering to the Raman intensity which was neglected in the previous study.¹⁹ After calculating the Raman amplitudes of the ERS and the phonon spectra, we found that the interference between the ERS and the phonon spectra gives a drastic change in the constructive-destructive interference near the phonon spectra, giving an asymmetry to the phonon lineshape when fitted to the BWF lineshape. By considering the second-order Raman process, we systematically reproduce the E_F dependence of the Raman spectra of graphene that was observed in experiment.⁹

Our paper is organized as follows. In Sec. II we describe our calculation of the electron-electron interaction using the TB method and considering up to second-order Raman processes. In Sec. III, we discuss the calculated ERS spectra as a function of E_F and compare the asymmetric BWF factor $1/q_{\text{BWF}}$ obtained from our calculation with that from the experiment. Finally, in Sec. IV we give a summary of this work.

II. THEORETICAL METHODS

The possible ERS processes are described in Fig. 1, which consist of either intravalley (A) or intervalley (E) interaction, either intravalley (a) or intervalley (e) scattering and either zero momentum transfer ($\mathbf{q} = 0$ first-order) or non-zero momentum transfer ($\mathbf{q} \neq 0$ second-order) processes.¹⁹ When a photon with the laser excitation energy E_L is introduced to the graphene sample, the photon excites an electron from an initial state i to an intermediate state n with an energy matched to E_L (incident resonance). This photoexcited electron (PE) is then scattered to another intermediate state n' by the Dirac electrons (DEs) on the Dirac cone and the electron finally recombines with a hole by emitting a scattered photon energy E_s as shown in Fig. 1. The Coulomb interaction between the PE and the DEs causes the PE to reduce its energy and changes PE's momentum while the DEs are being excited.

The number of DEs to be excited for each process depends on the number of the scattering order. In the first-order process, only one DE is excited and this process requires a zero momentum transfer ($\mathbf{q} = 0$) since the PE momentum (\mathbf{k}) should be the same as its hole

momentum in order to emit a scattered photon with energy E_s by the electron-hole recombination process. In the second-order process, on the other hand, the PE is scattered twice ($\mathbf{k} \rightarrow \mathbf{k} - \mathbf{q}$) and ($\mathbf{k} - \mathbf{q} \rightarrow \mathbf{k}$) and the PE excites two DEs with relative non-zero electron-hole momenta $-\mathbf{q}$ and \mathbf{q} . Due to the degeneracy of the Dirac cone at the K and K' points of the graphene Brillouin zone (BZ), both the first-order processes and the second-order processes may occur in the intravalley (A) interactions or in the intervalley (E) interactions. In the A interactions, the DEs are excited on the same Dirac cone as the PE, while in the E interactions, the DEs are excited on the other Dirac cone. In the case of the E interaction, the initial and final states of the PE and DEs can be in the same (different) valley which is defined by intravalley (intervalley) scattering labelled by a small letter “a” (“e”). The e scattering is not possible in the A interaction because $+\mathbf{q}$ and $-\mathbf{q}$ scattering are pointing to two different directions at the high symmetry points of graphene; one is pointing to the $\overline{\text{KK}}'$ direction while the other is pointing to the $\overline{\text{K}\Gamma}$ direction. Thus the Ae interaction does not conserve energy during the scattering processes. Combining all possible A and E interactions with the a and e scatterings we have: an Aa [Fig. 1(a)] and an Ea [Fig. 1(b)] in the first-order processes; and an Aa [Fig. 1(c)], an Ea [Fig. 1(d)], and an Ee [Fig. 1(e)] in the second-order processes.

The BWF asymmetry comes from the interference effect mentioned above because both the ERS and the phonon spectra have the same initial and final states for a single PE. Based on this standpoint, we define the Raman intensity:

$$I(\omega_s) = [A_G(\omega_s) + A_{\text{ERS}}(\omega_s)]^2, \quad (2)$$

where $A_G = \sum_{\nu} A_{\nu}$, in which A_{ν} and A_{ERS} are, respectively, the ν -th phonon scattering amplitude and the ERS scattering amplitude. The phonon scattering amplitude in the resonance Raman spectra is given by²¹

$$\begin{aligned} A_{\nu}(\omega_s) = & \frac{1}{\pi} \sum_{n,n'} \left[\frac{\mathcal{M}_{\text{el-op}}^{n,i}}{[\Delta E_{ni} - i\gamma]} \right. \\ & \times \frac{\mathcal{M}_{\text{el-}\nu}^{n',n}}{[\Delta E_{n'i} - \hbar\omega_G - i(\gamma + \Gamma_{\nu})]} \\ & \left. \times \frac{\mathcal{M}_{\text{el-op}}^{f,n'}}{[E_L - \hbar\omega_G - \hbar\omega_s - i\Gamma_{\nu}]} \right], \end{aligned} \quad (3)$$

where for the phonon modes we only consider the first-order process $\nu = \text{iTO}$ or LO modes, and $\Delta E_{ni} = E_L - E_n - E_i$. Here we use a broadening factor $\gamma = 0.1$ eV, which is related to

the inverse of the life time of the photoexcited carriers. On the other hand, Γ_ν is related to the life time of the electron-phonon interaction.²²

The values of Γ_ν and ω_G are considered as follows. In the gate-modulated Raman spectra, we expect phonon frequency softening and spectral broadening as we shift the Fermi energy from $|E_F| > 0$ to $E_F = 0$. This effect is due to the Kohn anomaly, i.e. renormalization of the phonon energy by electron-hole pair excitation in the G mode Raman spectra of graphene.⁴ We do not consider the Kohn anomaly effect explicitly in this calculation, but we can fit the peak position $\omega_G = 1591 + 15|E_F| \text{ cm}^{-1}$ for $-0.20 \leq E_F \leq 0.00 \text{ eV}$ and $\omega_G = 1591 + 22.5|E_F| \text{ cm}^{-1}$ for $0.00 < E_F \leq 0.40 \text{ eV}$. The inverse of the phonon life time is also fitted by $\Gamma_\nu = 5 - 10|E_F| \text{ cm}^{-1}$ for $-0.20 \leq E_F < 0.25 \text{ eV}$ and $\Gamma_\nu = 2.5 \text{ cm}^{-1}$ for $0.25 \leq E_F \leq 0.40 \text{ eV}$ so as to reproduce the experimental results.⁹ It is important to note that the Kohn anomaly does not give the asymmetric BWF of the G band spectra because the Kohn anomaly is not an interference phenomenon; only the interference effect between the G band and the ERS does however show a BWF lineshape. The electron-photon ($\mathcal{M}_{\text{el-op}}^{b,a}$) and electron-phonon ($\mathcal{M}_{\text{el-}\nu}^{b,a}$) matrix elements for a transition between states $a \rightarrow b$ are adopted from previous works within the TB method.^{23,24} We approximate the intermediate states (virtual states) to become a real state with $n = n'$, which is a good approximation for the resonance condition.²⁵

The ERS amplitude A_{ERS} is the summation of the amplitude from the first-order $A_{\text{ERS}}^{(1)}$ and second-order $A_{\text{ERS}}^{(2)}$ processes. The amplitude of the first-order ERS process is given by

$$A_{\text{ERS}}^{(1)}(\omega_s) = \frac{1}{\pi} \sum_{n,n'} \sum_{l,l'} \left[\frac{\mathcal{M}_{\text{el-op}}^{n,i}}{[\Delta E_{ni} - i\gamma]} \times \frac{K_{n',l',n,l}(0)}{[\Delta E_{n'i} - \hbar\omega_e - i(\gamma + \Gamma_e)]} \times \frac{\mathcal{M}_{\text{el-op}}^{f,n'}}{[E_L - \hbar\omega_e - \hbar\omega_s - i\Gamma_e]} \right], \quad (4)$$

where ω_e and $\Gamma_e = 30 \text{ meV}$ are, respectively, the energy of the excited DE electron and the inverse life time of the electron-electron interaction. The electron-electron interaction $K_{1,2,3,4}(\mathbf{q})$ defines the scattering of the PE [DE] from an initial state (1) [(2)] to a final state (3) [(4)] which consists of direct (K^d) and exchange (K^x) interaction terms,

$$K_{1,2,3,4}(\mathbf{q}) = K_{1,2,3,4}^d(\mathbf{q}) + K_{1,2,3,4}^x(\mathbf{q}), \quad (5)$$

for a spin singlet state. We do not consider spin triplet states for simplicity due to the fact

that the exchange interaction is sufficiently small.^{19,25} The direct $K_{1,2,3,4}^d(\mathbf{q})$ and exchange $K_{1,2,3,4}^x(\mathbf{q})$ Coulomb interactions between two electrons in the TB approximation is given by

$$K_{1,2,3,4}^d(\mathbf{q}) = \sum_{ss'=A,B} C_s^1 C_{s'}^2 C_s^{*3} C_{s'}^{*4} \text{Re}[v_{ss'}(\mathbf{q})], \quad (6)$$

$$K_{1,2,3,4}^x(\mathbf{q}) = \sum_{ss'=A,B} C_s^1 C_{s'}^2 C_{s'}^{*3} C_s^{*4} \text{Re}[v_{ss'}(\mathbf{k}' - \mathbf{k} - \mathbf{q})], \quad (7)$$

where $[1, 2, 3, 4] = [\mathbf{k}c, \mathbf{k}'v, (\mathbf{k} - \mathbf{q})c, (\mathbf{k}' + \mathbf{q})c]$ in the case of ERS in undoped-graphene ($E_F = 0$) [Fig. 2(a)]. In the electron doped ($E_F > 0$) and the hole doped ($E_F < 0$) cases, we add possible intraband transitions $[2, 4] = [\mathbf{k}'c, (\mathbf{k}' + \mathbf{q})c]$ and $[2, 4] = [\mathbf{k}'v, (\mathbf{k}' + \mathbf{q})v]$, respectively, as long as state (2) is occupied and state (4) is unoccupied. C_s^j is a tight binding coefficient for an atomic site $s = A, B$ and a state j .²⁶ The Fourier transform of the Coulomb potential $v_{ss'}(\mathbf{q})$ is defined by

$$v_{ss'}(\mathbf{q}) = \frac{1}{N} \sum_{u'} e^{i\mathbf{q} \cdot (\mathbf{R}_{u's'} - \mathbf{R}_{0s})} v(\mathbf{R}_{0s}, \mathbf{R}_{u's'}), \quad (8)$$

where $v(\mathbf{R}, \mathbf{R}')$ is the effective Coulomb potential for the π electron system modeled by the Ohno potential^{25,27}

$$v(\mathbf{R}, \mathbf{R}') = \frac{U_0}{\sqrt{\left(\frac{4\pi\epsilon_0}{e^2} U_0 |\mathbf{R} - \mathbf{R}'|\right)^2 + 1}}, \quad (9)$$

in which U_0 is the on-site Coulomb potential for two π electrons at the same site $\mathbf{R} = \mathbf{R}'$, defined by

$$U_0 = \int d\mathbf{r} d\mathbf{r}' \frac{e^2}{|\mathbf{r} - \mathbf{r}'|} \phi_\pi^2(\mathbf{r}) \phi_\pi^2(\mathbf{r}') = 11.3 \text{ eV}. \quad (10)$$

The amplitude of the second-order ERS process is given by

$$\begin{aligned} A_{\text{ERS}}(\omega_s) = & \frac{1}{\pi} \sum_{n,n',n''} \sum_{m,m',l,l'} \left[\frac{\mathcal{M}_{\text{el-op}}^{n,i}}{[\Delta E_{ni} - i\gamma]} \right. \\ & \times \frac{K_{n',m',n,m}^d(\mathbf{q})}{[\Delta E_{n'i} - \hbar\omega_1 - i(\gamma + \Gamma_e)]} \\ & \times \frac{K_{n'',l',n',l}^d(-\mathbf{q})}{[\Delta E_{n''i} - \hbar\omega_1 - \hbar\omega_2 - i(\gamma + 2\Gamma_e)]} \\ & \left. \times \frac{\mathcal{M}_{\text{el-op}}^{f,n'}}{[E_L - \hbar\omega_1 - \hbar\omega_2 - \hbar\omega_s - 2i\Gamma_e]} \right], \quad (11) \end{aligned}$$

where we also consider the same virtual state approximation as in Eq. (3). Here, ω_1 and ω_2 are the energies of the DEs emitted for the electron-electron interaction in the second-order ERS process.

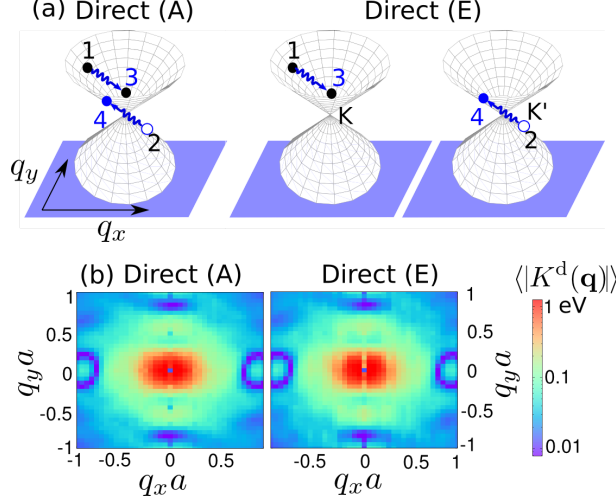


Figure 2: (Color online) (a) Illustration of the direct Coulomb intravalley (A) interaction and intervalley (E) interaction. (b) The averaged absolute value of the direct Coulomb interaction matrix element K^d as a function of momentum transfer \mathbf{q} for the intravalley (A) interaction and intervalley (E) interaction. The intervalley (e) scattering is not shown in this figure.

III. ELECTRONIC RAMAN SPECTRA AND THE BWF ASYMMETRY

Since the electron-electron interaction depends on initial states (1, 2) of PE and DE and also on a momentum transfer (\mathbf{q}), we consider the absolute average value of the matrix elements over the initial states in order to visualize the strength of the electron-electron interaction in a simple manner. The direct Coulomb interaction can occur in either the A or E interaction as shown in Fig. 2(a). Figure 2(b) depicts the absolute average value of $K_{1,2,3,4}^d(\mathbf{q})$ over the initial states (1, 2)

$$\langle |K_\mu^d(\mathbf{q})| \rangle = \frac{1}{N_1 N_2} \sum_{(1,2)} |K_{1,2,3,4}^d(\mathbf{q})|, \quad (12)$$

where $\mu = A$ and E . The e scattering is not shown in Fig. 2(b) for convenient comparison between the A and E interaction, since the A interaction does not have the e scattering. $\langle |K_\mu^d(\mathbf{q})| \rangle$ only depends on \mathbf{q} after taking the summation over the initial states (1, 2) because the final states (3, 4) depend on (1, 2) by momentum conservation in Eq. (6). As shown in Fig. 2(b), for both the A and E interactions, K^d disappears at $\mathbf{q} = 0$, indicated by a small dot at $\mathbf{q} = (0,0)$, due to the symmetry of the A and B sublattice wavefunctions in the graphene unit cell which cancel in the summation of K^d in Eq. (6).¹⁹ The absence of the direct Coulomb interaction suggests that the ERS should come from the second order $\mathbf{q} \neq 0$

electron-electron interaction, similar to what we found in m-SWNTs.¹⁹ The first-order ERS can only be possible by means of the exchange Coulomb interaction. Although we take into account the exchange Coulomb interaction, the Raman intensity from the first-order process is still six-orders of magnitude smaller than that of the second order process [see inset of Fig. 3(a)]. Therefore, we can neglect the first-order processes for both the A and E interactions.

In Fig. 3 we present the Raman intensity calculation $I(\omega_s)$ of Eq. (2). The solid curve in Fig. 3(a) shows the total Raman intensity after considering the interference of the G mode spectra with the ERS spectra, while the dashed line shows the Lorentzian G phonon spectra by taking the square of its probability amplitudes $A_G(\omega_s)$ [Eq. (3)]. The G mode constituents, i.e. the iTO and LO modes, are indicated by a dotted line and a dot-dashed line, respectively. It is clear from Fig. 3(a) that the calculated Raman spectra shows asymmetry around the peak position at 1590 cm^{-1} . By fitting the calculated result to Eq. (1), we obtain the fitted values of $1/q_{\text{BWF}}$, which have the same negative sign as the experimental data.⁹ For a negative $1/q_{\text{BWF}}$, when ω_s is smaller (greater) than ω_G , $I(\omega_s)$ is greater (smaller) than $|A_G(\omega_s)|^2$, indicating that the interference between the G mode and the ERS spectra is constructive (destructive) below (above) the resonance condition $\omega_s = \omega_G$.

By decreasing (increasing) E_F further from the Dirac cone, transitions from (to) the unoccupied (occupied) states are suppressed due to the Pauli principle. Thus we expect that the asymmetric factor $1/q_{\text{BWF}}$ decreases as we change the E_F from the Dirac point $E_F = 0.00\text{ eV}$ to $E_F = 0.20\text{ eV}$ as shown in Fig. 3(b). The solid line is the intensity of the spectrum with $1/q_{\text{BWF}} = -0.073$ when $E_F = 0.00\text{ eV}$, while the dashed line is the corresponding curve with $1/q_{\text{BWF}} = -0.043$ when $E_F = 0.20\text{ eV}$. The Raman intensity and peak position at $E_F = 0.20\text{ eV}$ are larger than that at $E_F = 0.00\text{ eV}$ due to the Kohn anomaly effect.⁴

Unlike the ERS spectra in m-SWNTs which are Lorentzian functions,^{18,19} the ERS intensity in graphene is a linear function of ω_s [inset of Fig. 3(b)]. The positive gradient of the ERS intensity is due to the greater scattering path available to excite DEs in the second-order processes as ω_s increases. The ERS intensity will increase monotonically and will get saturated at $\omega_s \geq E_L/2$. The absence of the ERS peak intensity in graphene is related to the absence of van-Hove singularities within the G mode energy $\sim 0.2\text{ eV}$ to $E_L = 2.4\text{ eV}$. The absence of the ERS peak also becomes the reason why the $1/q_{\text{BWF}}$ values of the G

mode in graphene are one-order of magnitude smaller compared to that in m-SWNTs. The ERS intensity is about two-orders of magnitude smaller than that of the G mode, and by increasing the E_F the ERS intensity decreases only less than 1%; nevertheless the change of the $1/q_{\text{BWF}}$ is significant [Fig. 3(b)]. Thus, this BWF feature is very sensitive to the presence or absence of the continuum spectra.

In Figures 4(a) and (b), we respectively show our calculated result and corresponding experimental results (Ref. 9) of the G band Raman intensity as a function of Raman shift, which is plotted for various values of E_F in the range $-0.20 \leq E_F \leq 0.40$ eV. In the original version,⁹ Fig. 4(b) was given as a function of gate voltages V_G . For our purpose of comparing the calculated results and experimental results, here we convert V_G to E_F using the relation $E_F = \text{sign}(V_G - V_0)\hbar v_F \sqrt{\alpha\pi|V_G - V_0|}$ where the Fermi velocity $v_F = 10^8$ cm/s, the constant voltage adjusted to the Dirac point $V_0 = -57.5$ V, and the capacitance $\alpha = 7.2 \times 10^{10}$ cm⁻²V⁻¹ for the SiO₂ dielectric medium with a thickness 300 nm.^{9,17,28} At the charge neutrality point $E_F = 0.00$ eV, the G band spectrum is broadened and its frequency is softened due to the Kohn anomaly effect. Comparison of the BWF asymmetric factor $1/q_{\text{BWF}}$ between the theory (square) and experiment (circle) shows a reasonable agreement in Fig. 4(c) except for $E_F \geq 0.20$ eV, when the experimental results deviate from the calculated results. We suppose that the deviation is related to the difficulties of observing the BWF asymmetry at $E_F > 0.20$ eV in the experiment because the continuum ERS intensity is about two or three-orders of magnitude smaller compared to the G band intensity. Such weak ERS spectra might couple strongly with the background spectra in the experiment which make it difficult to observe. The calculated asymmetric factor $1/q_{\text{BWF}}$ has a “V”-shaped curve structure as a function of E_F with the dip position at $E_F = 0.00$ eV. The decrease of $1/q_{\text{BWF}}$ is related to the decrease of the ERS intensity due to the suppression of electron-hole pair excitations on the Dirac cone upon doping.

The present agreement also reconfirms that plasmons do not contribute to the continuum spectra. The reason is as follows. When $|E_F| > 0$, collective excitations (plasmons) are expected to be generated, and consequently the ERS spectra should be enhanced.²⁹ However, what we obtain in the present study is that the ERS spectra are in fact suppressed if we increase $|E_F|$. Therefore, we rule out the contribution of plasmons in the ERS spectra and we conclude that only single-particle electron-hole pair excitations are important.

IV. SUMMARY

We show that the origin of the BWF spectra in graphene comes from the continuum single particle electron-hole pair ERS spectra interfering with the discrete G band phonon spectra. After calculating the Raman amplitudes of the ERS and the phonon spectra, we found that the interference effect between the ERS and the phonon spectra gives a drastic change in the constructive-destructive interference near the phonon resonance condition, leading to an asymmetry of the phonon lineshape when fitted to the BWF lineshape. By considering the second-order Raman process, we are able to reproduce the E_F dependence of the Raman spectra systematically. We expect that the asymmetric BWF feature appears generally in the phonon Raman spectra of all Dirac cone systems.

Acknowledgments

The authors are grateful to Duhee Yoon for sharing information regarding his gate-modulated Raman spectroscopy experiment (Ref. 9). E.H. is supported by a MEXT scholarship. A.R.T.N. acknowledges a JSPS research fellowship for young scientists No. 201303921. R.S. acknowledges MEXT Grants No. 25286005 and No. 225107004. M.S.D. acknowledges NSF-DMR Grant No. 10-04147.

* Electronic Address: hasdeo@flex.phys.tohoku.ac.jp

¹ L. M. Malard, J. Nilsson, D. C. Elias, J. C. Brant, F. Plentz, E. S. Alves, A. H. Castro Neto, and M. A. Pimenta, Phys. Rev. B **76**, 201401 (2007).

² D. L. Mafra, G. Samsonidze, L. M. Malard, D. C. Elias, J. C. Brant, F. Plentz, E. S. Alves, and M. A. Pimenta, Phys. Rev. B **76**, 233407 (2007).

³ M. Lazzeri, S. Piscanec, F. Mauri, A. C. Ferrari, and J. Robertson, Phys. Rev. B **73**, 155426 (2006).

⁴ S. Piscanec, M. Lazzeri, F. Mauri, A. C. Ferrari, and J. Robertson, Phys. Rev. Lett. **93**(18), 185503– (2004).

⁵ M.S. Dresselhaus, A. Jorio, and R. Saito, Annual Review of Condensed Matter Physics **1**, 89–108 (2010).

- ⁶ P. C. Eklund and K. R. Subbaswamy, Phys. Rev. B **20**, 5157–5161 (1979).
- ⁷ S. D. M. Brown, A. Jorio, P. Corio, M. S. Dresselhaus, G. Dresselhaus, R. Saito, and K. Kneipp, Phys. Rev. B **63**, 155414 (2001).
- ⁸ U. Fano, Phys. Rev. **124**, 1866–1878 (1961).
- ⁹ D. Yoon, D. Jeong, H. Lee, R. Saito, Y. Son, H. Lee, and H. Cheong, Carbon **61**, 373 – 378 (2013).
- ¹⁰ A. Jorio, M. S. Dresselhaus, R. Saito, and G. Dresselhaus. Raman Spectroscopy in Graphene Related Systems, Wiley, 2011.
- ¹¹ R. Saito, M. Hofmann, G. Dresselhaus, A. Jorio, and M. S. Dresselhaus, Advances in Physics **60**, 413–550 (2011).
- ¹² T. O. Wehling, H. P. Dahal, A. I. Lichtenstein, M. I. Katsnelson, H. C. Manoharan, and A. V. Balatsky, Phys. Rev. B **81**, 085413 (2010).
- ¹³ K. F. Mak, J. Shan, and T. F. Heinz, Phys. Rev. Lett. **106**, 046401 (2011).
- ¹⁴ D. Chae, T. Utikal, S. Weisenburger, H. Giessen, K. v. Klitzing, M. Lippitz, and J. Smet, Nano Letters **11**, 1379–1382 (2011).
- ¹⁵ A. B. Kuzmenko, I. Crassee, D. van der Marel, P. Blake, and K. S. Novoselov, Phys. Rev. B **80**(16), 165406 (2009).
- ¹⁶ T. Tang, Y. Zhang, C. Park, B. Geng, C. Girit, Z. Hao, M. C. Martin, A. Zettl, M. F. Crommie, S. G. Louie, Y. R. Shen, and F. Wang, Nat Nano **5**, 32 (2010).
- ¹⁷ R. Saito, K. Sato, P.T. Araujo, D.L. Mafra, and M.S. Dresselhaus, Solid State Communications **175-176**, 18–34 (2013).
- ¹⁸ H. Farhat, S. Berciaud, M. Kalbac, R. Saito, T. F. Heinz, M. S. Dresselhaus, and J. Kong, Phys. Rev. Lett. **107**, 157401 (2011).
- ¹⁹ E. H. Hasdeo, A. R. T. Nugraha, K. Sato, M. S. Dresselhaus, and R. Saito, Phys. Rev. B **88**, 115107 (2013).
- ²⁰ L. Yang, J. Deslippe, C.-H. Park, M. L. Cohen, and S. G. Louie, Phys. Rev. Lett. **103**, 186802 (2009).
- ²¹ P. Yu and M. Cardona. Fundamentals of semiconductors, physics and material properties, Springer, 2010.
- ²² K. Sato, R. Saito, A. R.T. Nugraha, and S. Maruyama, Chem. Phys. Lett. **497**, 94 – 98 (2010).
- ²³ J. Jiang, R. Saito, Ge. G. Samsonidze, S. G. Chou, A. Jorio, G. Dresselhaus, and M. S. Dres-

- selhaus, Phys. Rev. B **72**, 235408 (2005).
- ²⁴ A. Grüneis, R. Saito, Ge. G. Samsonidze, T. Kimura, M. A. Pimenta, A. Jorio, A. G. Souza Filho, G. Dresselhaus, and M. S. Dresselhaus, Phys. Rev. B **67**, 165402 (2003).
- ²⁵ J. Jiang, R. Saito, Ge. G. Samsonidze, A. Jorio, S. G. Chou, G. Dresselhaus, and M. S. Dresselhaus, Phys. Rev. B **75**, 035407 (2007).
- ²⁶ K. Sasaki and R. Saito, Prog. Theor. Phys. **176**, 253–278 (2008).
- ²⁷ V. Perebeinos, J. Tersoff, and P. Avouris, Phys. Rev. Lett. **92**, 257402 (2004).
- ²⁸ K. S. Novoselov, A. K. Geim, S. V. Morozov, D. Jiang, M. I. Katsnelson, I. V. Grigorieva, S. V. Dubonos, and A. A. Firsov, Science **306**, 666–669 (2004).
- ²⁹ E. H. Hwang and S. Das Sarma, Phys. Rev. B **75**, 205418 (2007).

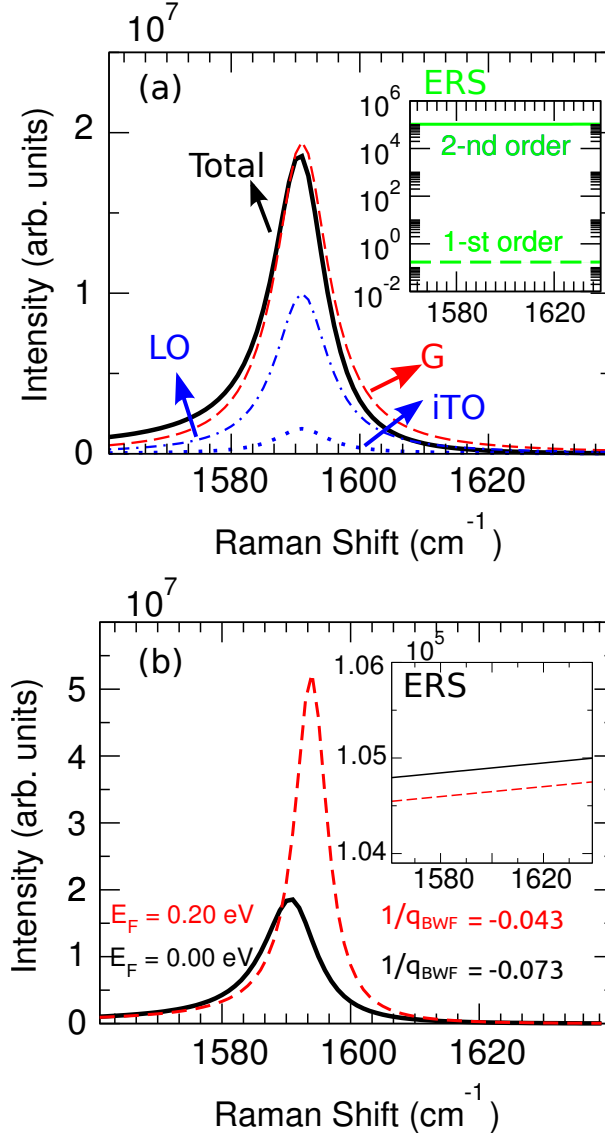


Figure 3: (Color online) (a) Calculated results of the total Raman intensity in Eq. (2) for $E_F = 0.00$ eV (solid line) compared with the Lorentzian G mode intensity by taking the square of A_G in Eq. (3) (dashed line). The G mode constituents, i.e. iTO and LO, are indicated by a dotted line and a dot-dashed line, respectively. An asymmetric lineshape (solid line) appears due to the interference effect of the G mode with the ERS. The inset shows calculated results of the first-order (dashed line) and the second-order (solid line) ERS spectra indicating that the second-order processes have an intensity value six-orders of magnitude greater than that of the first-order processes. (b) Calculated results of the total Raman intensity for $E_F = 0.00$ eV (solid line) and $E_F = 0.20$ eV (dashed line). The BWF asymmetric factor $1/q_{BWF}$ decreases by increasing the absolute value of $|E_F|$ away from the Dirac point because the ERS intensity also decreases by increasing $|E_F|$ (inset).

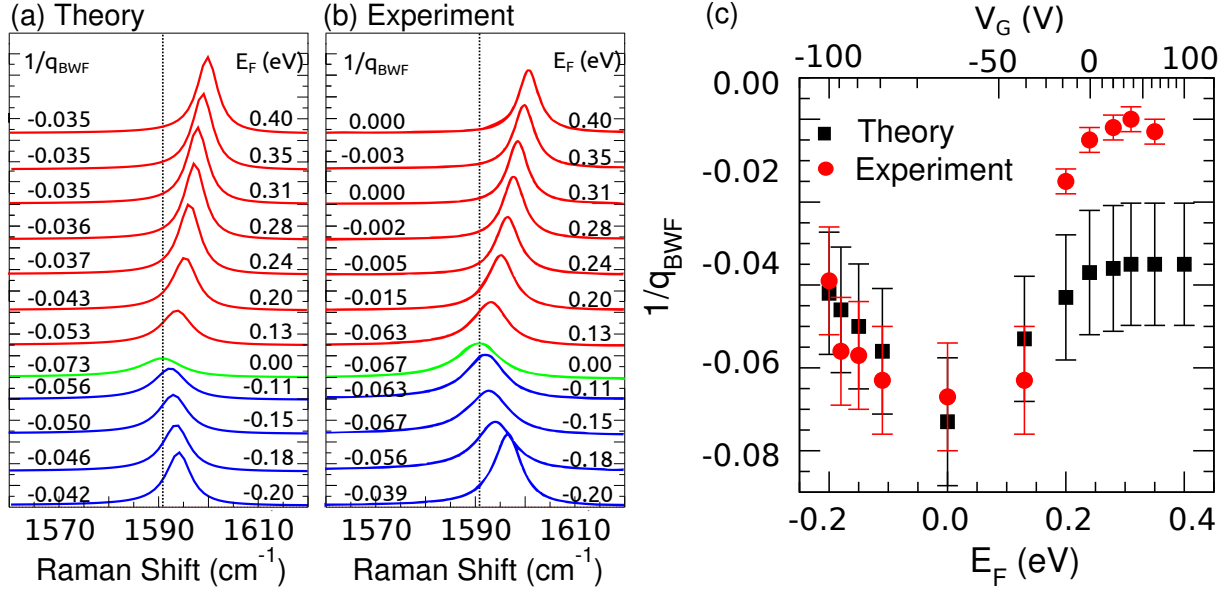


Figure 4: (Color online) Comparison between (a) the calculated results (this work) and (b) the experimental results taken from Ref. 9 for the *G* band Raman intensity as a function of Raman shift, which is plotted for various values of E_F in the range $-0.20 \leq E_F \leq 0.40$ eV. The values of $1/q_{\text{BWF}}$ obtained from the calculation and the experiment are also given on each plot. (c) Comparison of the BWF asymmetric factor $1/q_{\text{BWF}}$ as a function of E_F and gate voltage V_G between theory (squares) and experiment (circles). Both the linewidth and the phonon peak frequency-shift due to the Kohn anomaly effect are fitted from the experimental results in Ref. 9.